

Identification of a Novel Positron Emission Tomography (PET) Ligand for Imaging β -Site Amyloid Precursor Protein Cleaving Enzyme 1 (BACE-1) in Brain

Lei Zhang,^{*,†} Laigao Chen,[‡] Jason K. Dutra,[§] Elizabeth M. Beck,[†] Sangram Nag,^{||} Akihiro Takano,^{||} Nahid Amini,^{||} Ryosuke Arakawa,^{||} Michael A. Brodney,[†] Leanne M. Buzon,[§] Shawn D. Doran,[⊥] Lorraine F. Lanyon,[⊥] Timothy J. McCarthy,[‡] Kelly R. Bales,[#] Charles E. Nolan,[#] Brian T. O'Neill,[§] Klaas Schildknecht,[▽] Christer Halldin,^{||} and Anabella Villalobos[○]

[†]Medicine Design, Medicinal Chemistry, Pfizer Inc., Cambridge, Massachusetts 02139, United States

[‡]Clinical & Translational Imaging, Early Clinical Development, Pfizer Inc., Cambridge, Massachusetts 02139, United States

[§]Medicine Design, Medicinal Chemistry, Pfizer Inc., Groton, Connecticut 06340, United States

^{||}Department of Clinical Neuroscience, Center for Psychiatry Research, Karolinska Institutet and Stockholm County Council, SE-17176 Stockholm, Sweden

[⊥]Medicine Design, Pharmacokinetics, Dynamics and Metabolism, Pfizer Inc., Groton, Connecticut 06340, United States

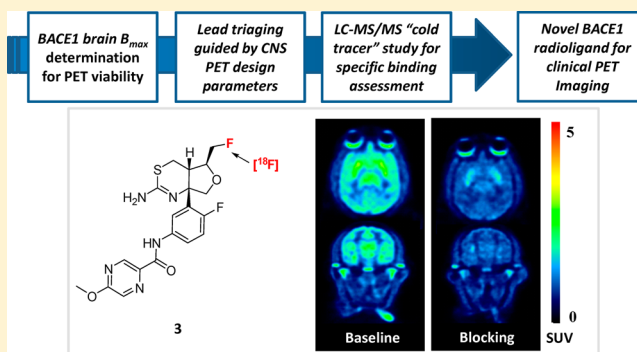
[#]Internal Medicine, Pfizer Inc., Cambridge, Massachusetts 02139, United States

[▽]Pharmaceutical Sciences, Pfizer Inc., Groton, Connecticut 06340, United States

[○]Medicinal Synthesis Technologies, Pfizer Inc., Groton, Connecticut 06340, United States

Supporting Information

ABSTRACT: Alzheimer's disease (AD) is characterized by accumulation of β -amyloid ($A\beta$) plaques and neurofibrillary tau tangles in the brain. β -Site amyloid precursor protein cleaving enzyme 1 (BACE1) plays a key role in the generation of $A\beta$ fragments via extracellular cleavage of the amyloid precursor protein (APP). We became interested in developing a BACE1 PET ligand to facilitate clinical assessment of BACE1 inhibitors and explore its potential in the profiling and selection of patients for AD trials. Using a set of PET ligand design parameters, compound 3 (PF-06684511) was rapidly identified as a lead with favorable in vitro attributes and structural handles for PET radiolabeling. Further evaluation in an LC-MS/MS "cold tracer" study in rodents revealed high specific binding to BACE1 in brain. Upon radiolabeling, [^{18}F]3 demonstrated favorable brain uptake and high in vivo specificity in nonhuman primate (NHP), suggesting its potential for imaging BACE1 in humans.



INTRODUCTION

Alzheimer's disease (AD) is a highly debilitating neurodegenerative disorder with significant unmet medical need for disease-modifying therapy.¹ During the past decade, the pharmaceutical industry has made significant investment on the advancement of potential disease-modifying therapies as evidenced by a number of clinical entries. However, the AD field as a whole has suffered from a high rate of clinical attrition² which may have been driven in part by the heterogeneous nature of patients enrolled in large and expensive phase II/III studies. In AD trials, patients have been typically recruited under broad diagnostic categories, a practice that may have led to a dilution in signals of clinical efficacy and inconclusive or negative trial outcomes. To help address this issue, clinical studies have recently started to

employ noninvasive positron emission tomography (PET) imaging agents to choose more homogeneous patient groups. As such, the use of PET ligands for $A\beta$ plaques³ and neurofibrillary tau tangles⁴ have become more routine in clinical trials, providing "PET imaging-based phenotypic signatures" and enabling better definition of optimal patient groups for late-stage clinical trials. As part of our BACE1 inhibitor program, we became interested in developing a BACE1-selective PET ligand to further enable clinical studies. A BACE1 PET ligand would serve as a valuable translational tool to help clinical characterization of BACE1 inhibitors by measuring in vivo target occupancy and its relationship to

Received: November 30, 2017

Published: January 22, 2018



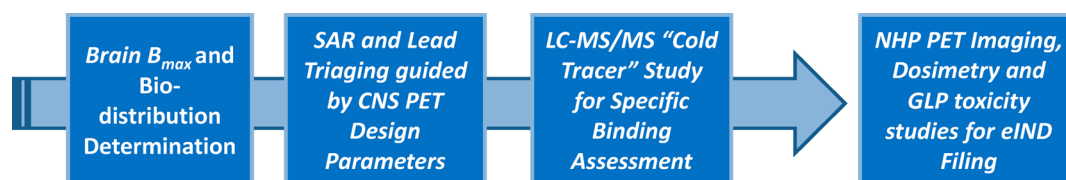


Figure 1. A rational and cost-effective CNS PET ligand discovery process.

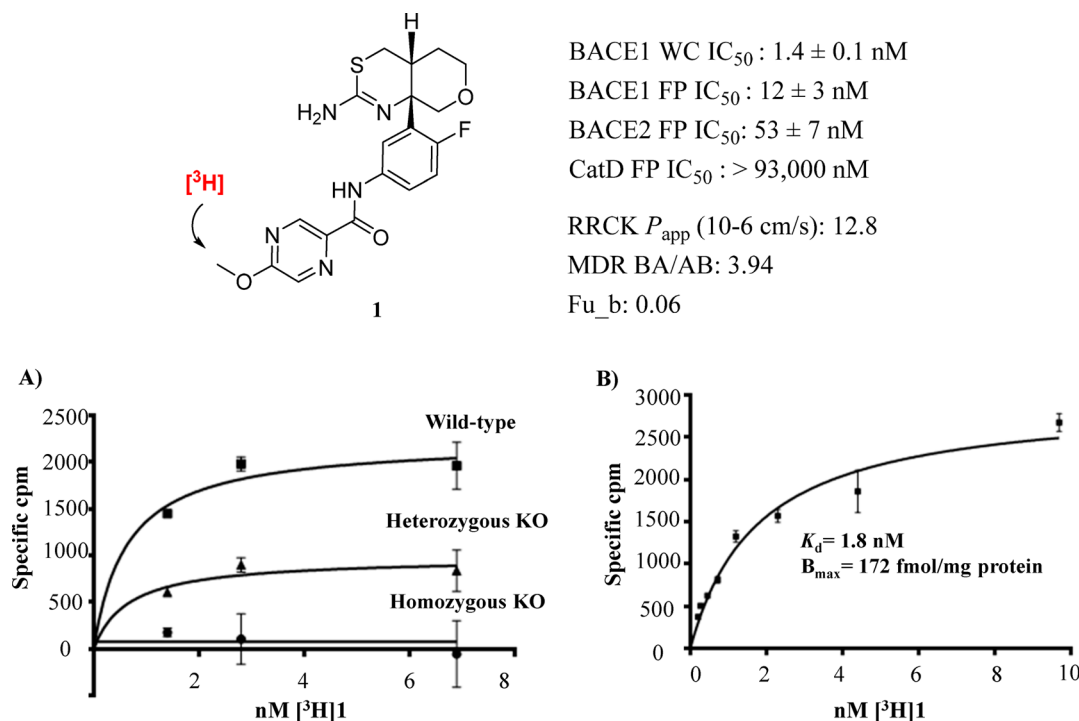


Figure 2. Profile of 1 and binding studies of [³H]1: (A) saturation binding of [³H]1 in brain frontal cortex homogenates of wild-type (WT), BACE1 heterozygous knockout (KO) and BACE1 homozygous KO mice; (B) BACE1 expression (B_{max}) and K_d determination in WT mice frontal cortex homogenate.

reduction of cerebrospinal fluid (CSF) A β levels. Furthermore, on the basis of reports that BACE1 enzyme level is elevated in AD brains,⁵ specifically in presynaptic dystrophic neurites surrounding amyloid plaques,⁶ we were keen to understand if the brain BACE1 enzyme levels of AD patients could be quantified by clinical PET imaging. Such information could in turn be combined with other biomarkers (e.g., amyloid plaque and tau imaging) to ultimately provide a more comprehensive understanding of AD etiology.

Development of BACE1 inhibitors has been a major effort across the pharmaceutical industry for over a decade, which has led to extensive literature disclosures featuring chemical matter with significant diversity in structure and properties.⁷ Our BACE1 PET efforts started with a survey of existing BACE1 inhibitor chemical matters from the literature and our internal effort. Identifying a potential PET ligand from existing chemical matter was greatly facilitated by using our central nervous system (CNS) PET ligand discovery process illustrated in Figure 1.⁸ As a first step in our PET ligand discovery effort, we sought to determine the maximum concentration of target binding sites (B_{max}) of BACE1 in brain early in the process to inform PET viability. Favorable BACE1 brain expression would trigger subsequent lead triaging, guided by a set of CNS PET design and selection criteria previously disclosed by our group.⁹ Specifically, compounds with the following attributes would be

prioritized: high BACE1 potency and selectivity, favorable physicochemical properties as measured by CNS PET multi-parameter optimization (MPO), fraction unbound in brain (Fu_b) > 0.05 for low risk of nonspecific binding (NSB), high passive permeability (RRCK P_{app} AB > 5×10^{-6} cm/s), and low P-glycoprotein (P-gp) transporter activity (MDR1 BA/AB ≤ 2.5) for brain permeability. PET ligand leads emerging from the triaging process would be assessed via a liquid chromatography–mass spectroscopy/mass spectroscopy (LC-MS/MS) “cold tracer” method¹⁰ in rodents for in vivo specific binding. Implementation of these steps would allow effective prioritization and make it possible to advance only one or two best PET leads into subsequent nonhuman primate (NHP) PET imaging and dosimetry studies, ultimately enabling clinical imaging of BACE1. Herein, we describe our efforts in the identification of [¹⁸F]PF-06684511 ([¹⁸F]3) as a promising PET ligand with favorable brain uptake and high specific binding to BACE1 in NHP via effective utilization of PET ligand design parameters and LC-MS/MS cold tracer method.

RESULTS AND DISCUSSION

BACE1 Brain Expression (B_{max}) Determinations. As part of our initial efforts in developing a PET ligand for BACE1, we were keen to identify a tool compound that could be tritiated and used for ex vivo saturation binding studies to determine

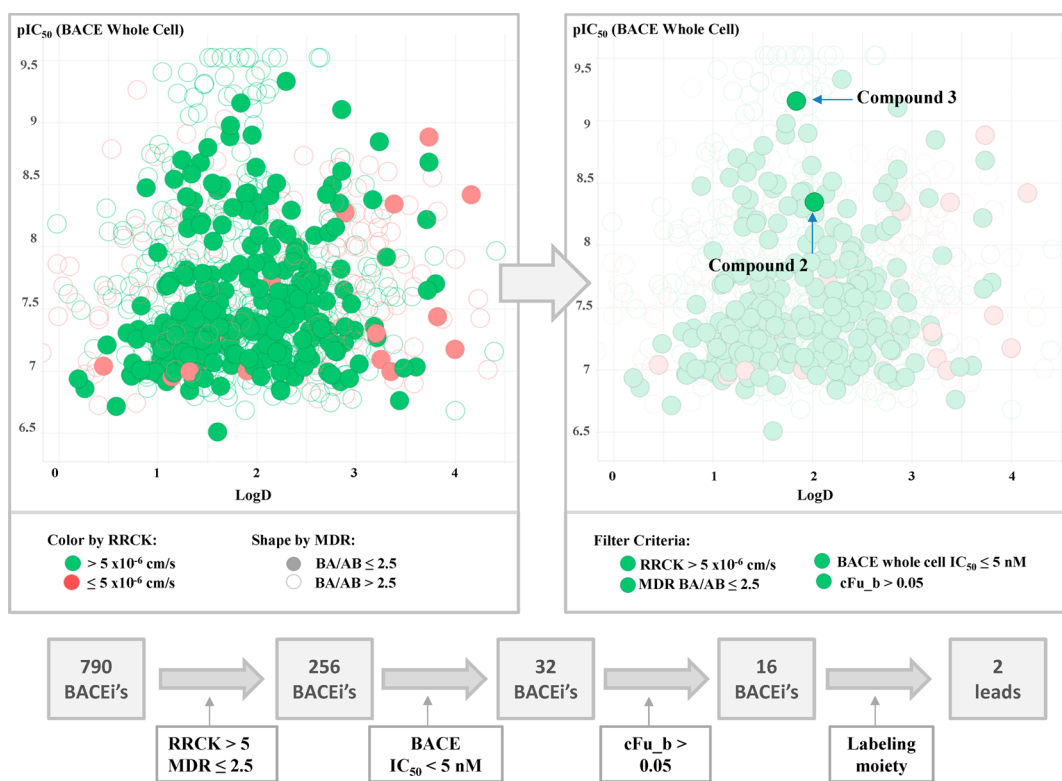


Figure 3. BACE1 PET ligand triaging based on CNS PET ligand design parameters.

BACE1 B_{\max} in brain tissue. It was necessary for such a tool compound to be potent and selective for BACE1 and have low NSB in brain tissue but not necessarily be brain permeable. Compound **1**, derived from a chemotype previously reported by Eisai,¹¹ caught our attention. As shown in Figure 2, compound **1** exhibited good potency at BACE1 with a whole cell IC_{50} of 1.4 nM and a cell-free fluorescence polarization (FP) IC_{50} of 12 nM. While **1** did have limited selectivity (4.5 \times) over BACE2,¹² a BACE1 homologue protein, it demonstrated remarkable selectivity over cathepsin D (CatD) and other targets. As BACE2 is mainly expressed in peripheral tissues (e.g., kidney, pancreas, etc.) and has minimal expressions centrally,¹³ we anticipated that the BACE2 activity of compound **1** would not significantly interfere with the determination of BACE1 B_{\max} in brain. Properties such as low lipophilicity (eLogD = 1.1) and fraction unbound in brain (Fu_b = 0.06) suggested a low risk of NSB. Compound **1** displayed moderate transporter activity (MDR1 BA/AB = 3.94), however, it is fit-for-purpose for ex vivo saturation binding studies in brain tissue where brain permeability is not required. Structurally, compound **1** bears a methoxy group amenable for tritiation. The 3H -labeling of **1** was readily achieved via alkylation of the corresponding hydroxyl pyrazine precursor **5** with $[^3H]CH_3I$ (Chemistry section, Scheme 1).

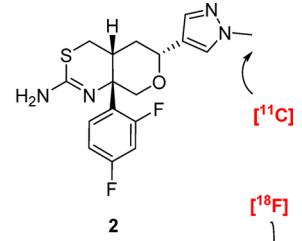
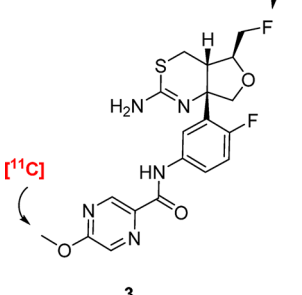
With $[^3H]$ **1** in hand, we carried out saturation binding studies in mouse brain tissue to understand the level of BACE1 brain expression. It is well-known that BACE1 is expressed throughout various brain regions.¹⁴ The mouse frontal cortex brain homogenate was used as a representative brain region for B_{\max} determination. We first carried out binding studies with $[^3H]$ **1** (vehicle + 3 dosing groups) in wild-type (WT) as well as BACE1 heterozygous and homozygous knockout (KO) mouse frontal cortex tissues to confirm its BACE1 specificity in brain and minimum interference due to its BACE2 activity. We were

gratified to see that different levels of specific binding of $[^3H]$ **1** indeed were observed (Figure 2A). The highest brain binding was seen in WT mice, which was reduced to roughly 50% in heterozygous BACE1 KO mice. Importantly, no specific binding was observed in homozygous BACE1 KO mice, confirming that even with comparable activity at BACE2, $[^3H]$ **1** only labeled BACE1 specifically in brain, likely due to low brain expression of BACE2. These results boosted our confidence in the B_{\max} value determined by this radiotracer as an accurate measure of BACE1 expression in brain. Subsequently, a thorough saturation binding (vehicle + 8 dosing groups) using WT frontal cortex homogenate (Figure 2B) yielded a K_d value of 1.8 nM, comparable to the in vitro whole cell (WC) potency, and a B_{\max} value of 144 fmol/mg protein (~ 7 nM assuming 50 mg protein/g wet tissue) residing in a range favorable for PET consideration. This B_{\max} value suggested that a potent compound, with WC IC_{50} most likely in the sub-nM range, would be desirable to achieve a favorable B_{\max}/K_d ratio > 10 , which is typically associated with successful PET ligands.¹⁵

PET Ligand Lead Triaging. With sufficient BACE1 expression in brain confirmed, we turned our attention to identifying suitable leads for PET consideration. Ideal candidates would retain the desired pharmacology, selectivity, and low NSB profile of **1** and, in addition, have high passive permeability and low transporter activities for better brain permeability. As shown in Figure 3, starting from roughly 800 BACE1 inhibitors (literature leads and internal Pfizer compounds), we quickly narrowed down the list to 256 compounds (represented by solid green circles) upon filtering by favorable MDR1 BA/AB (≤ 2.5) and RRCK ($> 5 \times 10^{-6}$ cm/s) values. Among these, 32 compounds displayed BACE1 WC IC_{50} values less than 5 nM. Further prioritization using calculated Fu_b¹⁶ (> 0.05) narrowed the list down to 16 compounds. From this cohort, compounds **2**¹⁷ and **3** (PF-

06684511, a compound previously reported by Eisai¹⁸) were chosen for further follow-up as they both had structure moieties amenable to either ¹¹C- or ¹⁸F-labeling. The pharmacology and PET-specific properties of compound 2 and 3 are shown in Table 1. In terms of pharmacology, compound 3 was the more potent of the two with sub-nM WC BACE1 IC₅₀ and around 15-fold selective over BACE2. Both compounds were highly selective against CatD and other targets in broad-spectrum CEREP selectivity panel evaluations. Compounds 2 and 3

Table 1. Pharmacology and Property Profile of BACE1 PET Ligand Leads 2 and 3 (PF-06684511)

		
	2	3
compd	2	3
Pharmacology		
BACE1 WC IC ₅₀ (nM) ^a	4 ± 0.5	0.7 ± 0.2
BACE1 FP IC ₅₀ (nM) ^b	53 ± 7	16 ± 2.3
BACE2 FP IC ₅₀ (nM) ^c	265 ± 32	239 ± 18
CatD FP IC ₅₀ (nM) ^d	13600 ± 3600	206000 ± 13000
Physicochemical Properties		
CNS PET MPO ^e	3.9	3.0
eLogD ^f	1.2	1.4
In Vitro PK Properties		
RRCK P _{app} AB (10 ⁻⁶ cm/s) ^g	17.7 ± 3	17.5 ± 2
MDR BA/AB ^h	1.92 ± 0.8	1.55 ± 0.7
cFu _b ⁱ	0.13	0.08

^aIC₅₀ values obtained from BACE1 whole cell (WC) assay; values represent the geometric mean of at least three experiments with standard error. ^bIC₅₀ values obtained from BACE1 cell free fluorescence polarization (FP) assay; values represent the geometric mean of at least three experiments with standard error. ^cIC₅₀ values obtained from BACE2 cell free FP assay; values represent the geometric mean of at least three experiments with standard error. ^dIC₅₀ values obtained from CatD cell free FP assay; values represent the geometric mean of at least three experiments with standard error. ^eCNS PET MPO represents the summation of scores of six commonly used individual physicochemical properties using the transformed functions described in ref 9. ^fExperimentally measured Log D using a reverse phase HPLC method.¹⁹ ^gRRCK cells with low transporter activity were isolated from Mardin–Darby canine kidney (MDCK) cells and were used to estimate passive permeability. ^hRatio from the MS-based quantification of P_{app,A→B} and P_{app,B→A} of the test compound (1 μM) across contiguous monolayers from MDR1-transfected MDCK cells; ⁱIn silico calculated fraction unbound in brain.

showed low lipophilicity (Log D < 2) and resided in favorable CNS drug space. Compound 3 had a slightly lower CNS PET MPO score, mainly due to a high number of H-bond donors. Nevertheless, both compounds displayed aligned in vitro ADME parameters for CNS PET ligand consideration, with low MDR1 efflux, high passive permeability and favorable calculated Fu_b (>0.05) suggesting low risk of NSB.

Prompted by their overall favorable profiles, 2 and 3 were further assessed for brain permeability in vivo. As shown in Table 2, both compounds demonstrated favorable measured

Table 2. Neuropharmacokinetic (NeuroPK) Profile of 2 and 3 in CD-1 Mice

compd	Fu _b ^a	mFu _p ^b	C _{p,u} (h·nM) AUC _{0–Tlast} ^c	C _{b,u} (h·nM) (AUC _{0–Tlast}) ^d	C _{b,u} /C _{p,u}
2	0.11	0.51	1321	701	0.53
3	0.06	0.25	718	321	0.45

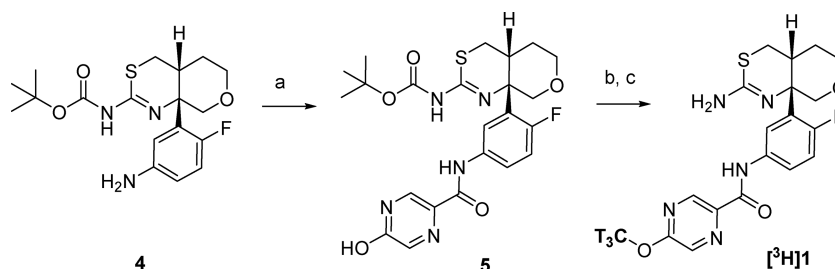
^aFraction unbound in brain homogenate.²⁰ ^bFraction unbound in mouse plasma. ^cAUC_{0–Tlast}-derived ratio of plasma unbound compound concentration in CD-1 mice (10 mg/kg PO). ^dAUC_{0–Tlast}-derived ratio of brain unbound compound concentration in CD-1 mice (10 mg/kg, PO).

fractions unbound in brain and plasma, confirming good alignment of experimental and in silico predicted values. Indeed, rodent neuropharmacokinetic studies showed favorable brain permeability with a free brain to plasma ratio (C_{b,u}/C_{p,u}) of 0.53 for compound 2 and 0.45 for compound 3.

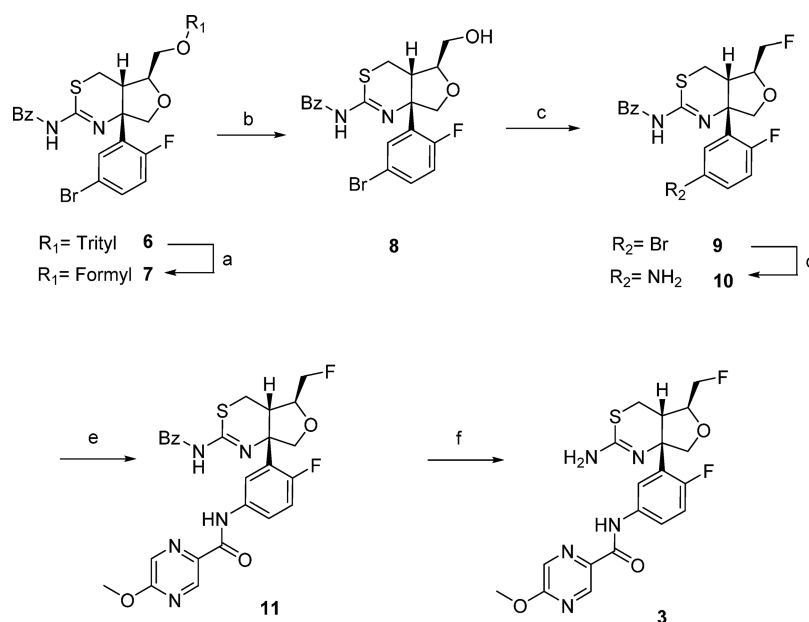
Chemistry. The tritiation of compound 1, illustrated in Scheme 1, started from a known aniline intermediate 4.¹¹ Amide coupling with 5-hydroxypyrazine 2-carboxylic acid yielded the hydroxyl pyrazine precursor 5. The subsequent methylation step was first explored using nonradioactive methyl iodide with anticipation of an O- versus N-alkylation selectivity challenge. Typical methylation conditions using cesium carbonate as base gave predominantly undesired N-methylation product. Changing the base to silver carbonate yielded a 1:1 mixture of the desired compound 1 and the N-methylation product that could be easily separated. Using this improved methylation condition and subsequent Boc removal, [³H]1 was obtained in high radiochemical purity (>99%) and specific radioactivity (80 Ci/mmol).

Our synthesis of 3 was accomplished from known intermediate 6²¹ using modified procedures from the literature (Scheme 2).²² The trityl group of 6 was removed through a two-step process involving solvolysis in formic acid to afford formate ester 7 and subsequent hydrolysis to provide alcohol 8. The fluoride group was then installed, at this early stage, by activation of alcohol 8 with perfluorobutanesulfonyl fluoride (NfF) to give intermediate 9. Introduction of the amide functionality was achieved by first converting the bromide of 9 to an azide via copper catalysis followed by concomitant reduction mediated by L-ascorbate to afford aniline 10.²³ The amide was then installed under standard coupling conditions using HATU to afford 11. Benzoyl deprotection in basic MeOH provided compound 3 with no amide cleavage observed.

For the preparation of the ¹⁸F-labeling precursor 18 (Scheme 3), we modified the synthesis used for 3 to enable a late-stage fluorination. As shown in Scheme 3, copper-catalyzed azide formation and subsequent in situ reduction by L-ascorbate converted intermediate 6 to the corresponding aniline 12.

Scheme 1^a

^aReagents and conditions: (a) 5-hydroxypyrazine-2-carboxylic acid, HBTU, DIPEA, DMF, rt, 34%; (b) [³H]CH₃I, Ag₂CO₃, CHCl₃, rt; (c) TFA, DCM, rt, 80 Ci/mmol specific activity, >99% radiochemical purity.

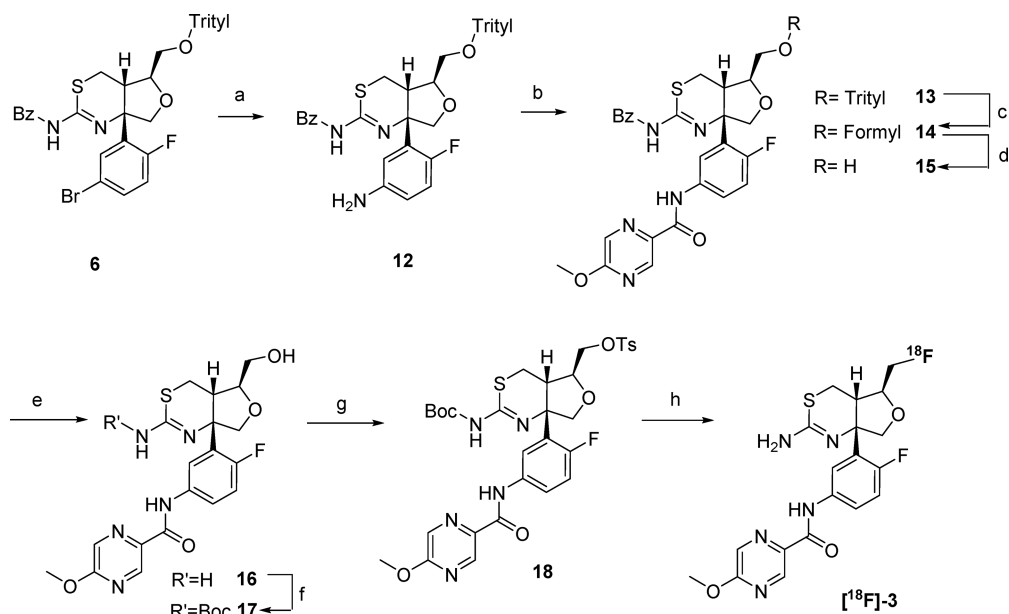
Scheme 2^a

^aReagents and conditions: (a) HCO₂H (neat), 0 °C to rt; (b) LiOH, THF/H₂O (1/1 v/v), rt; (c) perfluorobutanesulfonyl fluoride (NfF), Et₃N·3HF, Et₃N, THF, 0–40 °C, 52% for 3 steps; (d) NaN₃, *N,N'*-dimethylcyclohexane-1, 2-diamine, sodium L-ascorbate, CuI, EtOH/H₂O (3/1 v/v), 70 °C, 72%; (e) 5-methoxypyrazine-2-carboxylic acid, HATU, DIPEA, CH₃CN, rt, 93%; (f) DBU, MeOH, 60 °C, 77%.

Introduction of the amide was accomplished in the presence of propylphosphonic anhydride (T3P) to provide **13**. In preparation for the late-stage fluorination, the trityl group of **13** was removed in two steps involving formic acid solvolysis and base catalyzed hydrolysis to give intermediate **15**. To better accommodate the short half-life of ¹⁸F radionuclide (*T*_{1/2} = 110 min), we next carried out a protecting group exchange by first removing the benzoyl protecting group with DBU in MeOH to give **16**, followed by Boc-protection under standard conditions to give compound **17** in 58% yield over two steps. We expected that the eventual *t*-Boc removal would be mild and rapid under acidic conditions. Finally, tosylation of the hydroxyl group provided the desired labeling precursor **18** in good yields. ¹⁸F-Labeling proceeded by nucleophilic displacement of the tosyl group using [¹⁸F]fluoride/kryptofix 222 in DMSO, followed by rapid Boc-removal by aqueous HCl. Upon purification by semipreparative HPLC, [¹⁸F]**3** was generated in high radiochemical purity (>99%) and molar activity (84 and 175 GBq/μmol at the time of injection).

LC-MS/MS “Cold Tracer” Study in Rodents. As both compounds **2** and **3** demonstrated suitable PET properties and good brain permeability, we sought an early read for BACE1

specific binding to differentiate these two leads prior to triggering radiochemistry and PET imaging. Toward this end, we utilized a LC-MS/MS based “cold tracer” method,¹⁰ in which nonradioactive **2** and **3** were dosed intravenously in mice at tracer level (10 μg/kg). Concentrations in four brain regions (cerebellum, frontal cortex, hippocampus, and striatum) and plasma were quantified. As there is no reference region due to the widespread expression of BACE1 throughout the brain, we performed studies with baseline (vehicle) and blocking (pretreatment of a BACE1 selective inhibitor) arms to determine whether compound concentrations in the four main brain regions could be reduced as an indication of BACE1 specific binding. The results of the LC-MS/MS studies are illustrated in Figure 4. As shown in Figure 4A, no significant reduction in the concentration of **2** in the brain regions examined other than frontal cortex could be observed after pretreatment with a high dose of BACE1 inhibitor A²⁴ (100 mg/kg, SC), suggesting a lack of *in vivo* specific binding. In contrast, the concentration of **3** was dose dependently reduced in all four brain regions upon pretreatment of BACE1 inhibitor B²⁵ (1, 10, 80 mg/kg, SC, Figure 4B). To further validate that the specific binding of **3** was BACE1-driven, we further

Scheme 3^a

^aReagents and conditions: (a) NaN₃, *N,N'*-dimethylcyclohexane-1, 2-diamine, sodium L-ascorbate, CuI, EtOH/H₂O (3.5/1 v/v), 70 °C; (b) 5-methoxypyrazine-2-carboxylic acid, propane phosphonic acid anhydride (T3P), pyridine, DCM, rt, 41% over two steps; (c) HCO₂H (neat), 0 °C to rt; (d) LiOH, THF/H₂O (1/1 v/v), rt, quantitative yield; (e) DBU, MeOH, 60 °C; (f) Boc₂O, Et₃N, THF, 60 °C, 58% over two steps; (g) TsCl, DIPEA, DMAP, DCM, rt, 56%; (h) [¹⁸F]fluoride/kryptofix 222, DMSO, 150 °C, 5 min, followed by 1.5 M HCl, 100 °C, 3 min, 4% and 7% radiochemical yield (>99% purity), 187 and 417 MBq of delivered radioactivity, and 84 and 175 GBq/μmol of specific radioactivity at the time of injection.

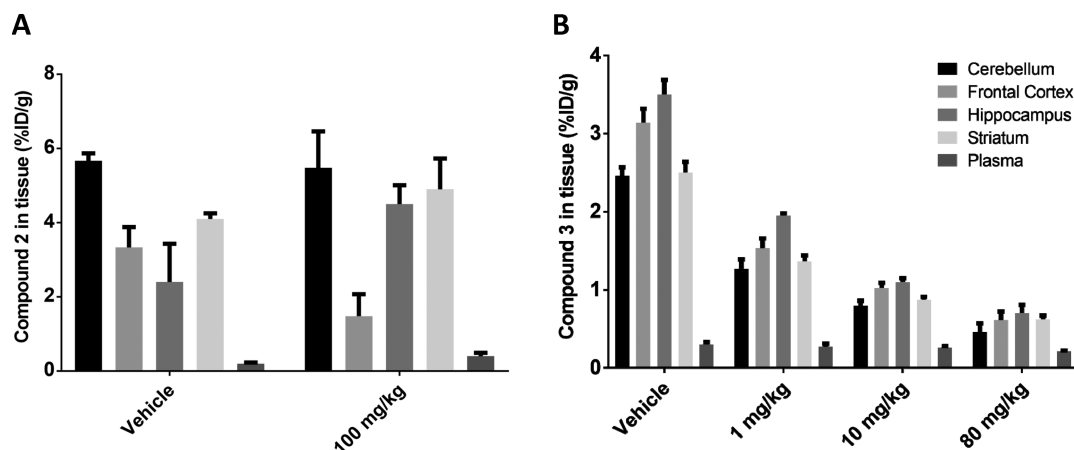


Figure 4. In vivo specific binding assessment of 2 and 3 in male 129/sve mice using LC-MS/MS “cold tracer” method. (A) Distribution of 2 in cerebellum, frontal cortex, hippocampus, striatum, and plasma, pretreated with either vehicle or BACE1 inhibitor A²² (100 mg/kg, SC) 60 min prior to ligand administration. (B) Distribution of 3 in cerebellum, frontal cortex, hippocampus, striatum, and plasma, pretreated with either vehicle or BACE1 inhibitor B²³ (1, 10, 80 mg/kg, SC) 60 min prior to ligand administration. For both studies, brain tissues and plasma were collected at 45 min post administration (*n* = 5 per animal group) at which the highest brain tissue/plasma ratios were achieved for 2 and 3 (see [Supporting Information](#), section 3).

examined the distribution of 3 in WT and BACE1 KO mice following the same protocol ([Figure 5](#)). We were gratified to see significant reduction in the concentration of 3 across the four brain regions of BACE1 KO mice compared to WT mice. These data indicated that compound 3 displayed the desired BACE1 specific binding in vivo and was a good candidate for further PET evaluation. While 2 had many desirable properties that met our PET ligand criteria, its potency may have not been sufficient to achieve specific binding in vivo.

NHP PET Imaging. The favorable binding profile of 3 in the LC-MS/MS “cold tracer” experiment prompted us to

advance this lead to subsequent radiochemistry and PET imaging studies. Radiofluorination of 3 was achieved in high radiochemical purity and delivered radioactivity as illustrated in [Scheme 3](#). The specific binding of [¹⁸F]3 was evaluated in NHP by PET under both baseline and blocking conditions. A total of two PET scans (one female NHP, one baseline scan, and one blocking scan) were performed with injected radioactivity of 154 and 117 MBq, specific radioactivities at the time of injection of 84 and 175 GBq/μmol, and injected mass of 0.8 and 0.3 μg. The summed PET images of baseline and blocking conditions, as well as the coregistered MRI image, of the NHP

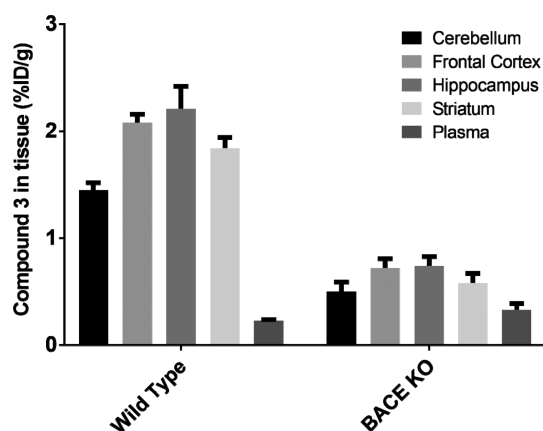


Figure 5. In vivo specific binding assessment of **3** in BACE1 WT and KO mice, using LC-MS/MS “cold tracer” method: four brain regions (cerebellum, frontal cortex, hippocampus, and striatum) and plasma were collected at 45 min post administration ($n = 5$ per animal group).

are shown in Figure 6. Consistent with LC-MS/MS study results, [^{18}F]**3** demonstrated good brain uptake and widespread distribution in various brain regions, with enriched signal in hippocampus and striatum (Figure 6B). The peak of the brain uptake reached at approximately 20 min and reduced to half at 120 min under baseline condition. In addition, upon administration of a BACE1 inhibitor (LY2886721, 26 5 mg/kg, PO, 2 h prior to PET scanning), the radio signal of [^{18}F]**3** decreased significantly (Figure 6C) across different brain regions (Figure 7), demonstrating BACE1 specificity.

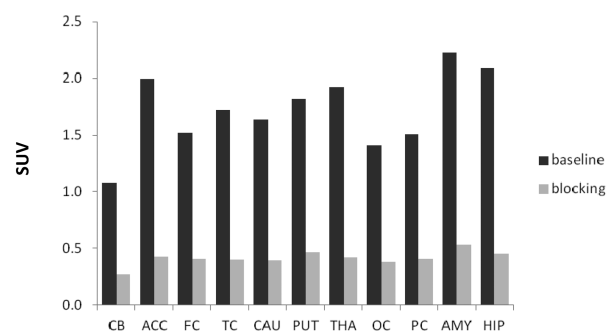


Figure 7. Standardized uptake values (SUVs) of [^{18}F]**3** in representative brain regions under baseline and blocking conditions. CB, cerebellum; ACC, anterior cingulate cortex; FC, frontal cortex; TC, temporal cortex; CAU, caudate; PUT, putamen; THA, thalamus; OC, occipital cortex; PC, parietal cortex; AMY, amygdala; HIP, hippocampus.

CONCLUSIONS

BACE1 is an aspartyl protease that plays a key role in the generation of $A\beta$ fragments via extracellular cleavage of the amyloid precursor protein (APP). BACE1 expression level has been reported to be elevated in AD patients. However, no BACE1 specific PET ligand has been reported to date, which allows in vivo quantification of BACE1 expression and target

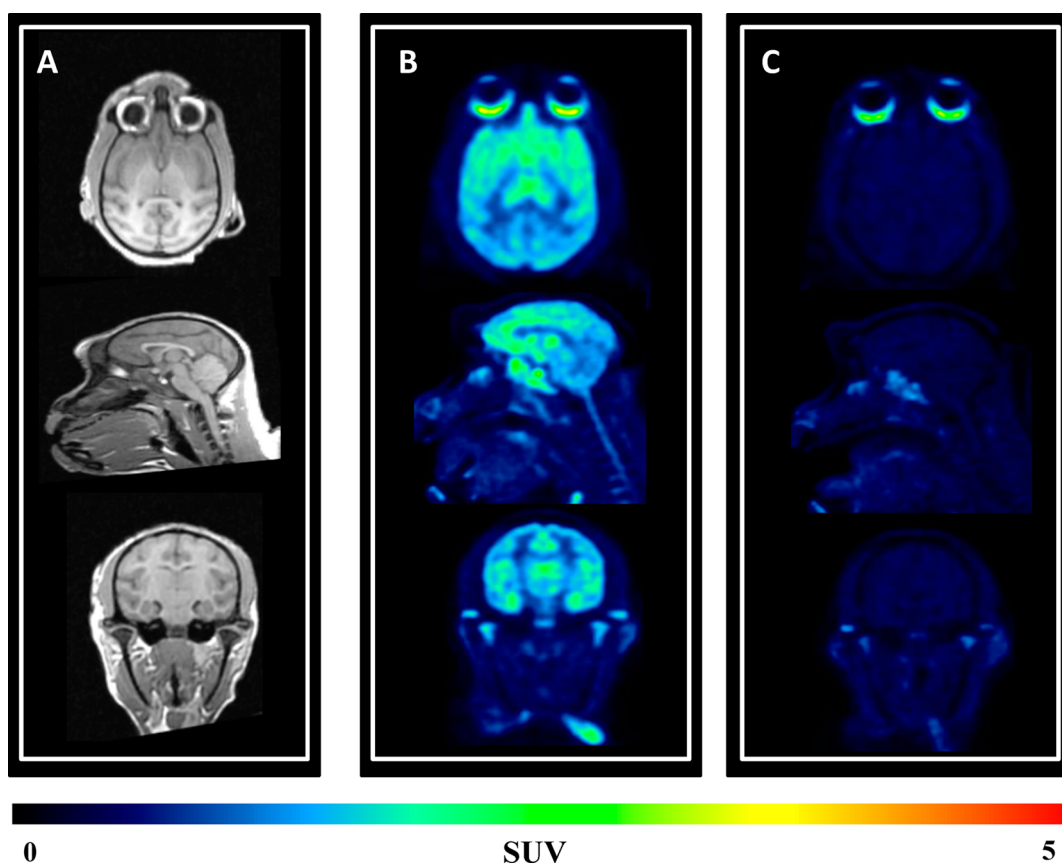


Figure 6. MRI (A) and PET images of [^{18}F]**3** in NHP summed from 32 to 180 min under (B) baseline and (C) blocking (pretreatment with a BACE1 inhibitor, LY2886721, 5 mg/kg, PO) conditions.

occupancy measurement. Through an efficient and cost-effective CNS PET ligand discovery process, we have successfully identified [^{18}F]3 as a novel PET ligand specific to BACE1 in brain.

As a first step, we determined B_{max} in brain tissue using an earlier non-brain penetrant radiotracer [^3H]1 and established the PET viability of this target. The PET ligand selection criteria previously reported by our group was applied to narrow an extensive collection of literature and in-house BACE1 inhibitors to just two leads, 2 and 3, based on key pharmacological, physicochemical, and ADME properties as well as structural amenability to ^{11}C - or ^{18}F - labeling. Prior to PET radiolabeling, these two leads were advanced into rodent LC-MS/MS “cold tracer” studies for specific binding evaluation, from which compound 3 emerged as a promising PET ligand lead with the desired level of BACE1 specific binding. The favorable outcome from the LC-MS/MS “cold tracer” studies successfully translated to NHP PET imaging, where [^{18}F]3 demonstrated excellent brain uptake and high BACE1 specific binding under baseline and blocking conditions. These results confirmed [^{18}F]3 as a suitable PET ligand for BACE1 PET imaging in vivo and reinforced the value of our overall PET discovery approach. This and previous work from our laboratories demonstrate that we have put in place a rational and cost-efficient paradigm for the development of novel PET ligands that can successfully identify a small number of candidate ligands ($n = 1\text{--}3$) from a large set of compounds.^{9,27}

We envision that BACE1 PET ligand [^{18}F]3 could facilitate the development of AD therapeutics in multiple ways. First, successful translation of this PET ligand to the clinic would enable target occupancy measurement of clinical BACE1 inhibitors and relationship of target occupancy to reduction of $\text{A}\beta$ levels in CSF. Furthermore, [^{18}F]3 could enable the examination of brain BACE1 enzyme levels in AD patients across the disease continuum. A robust correlation of BACE1 level with AD progression would render this BACE1 PET ligand as a valuable AD biomarker, which in turn could be used in conjunction with other established imaging-based AD biomarkers, such as amyloid plaque and tau PET imaging as well as hippocampus volume, to enable a deeper understanding of AD etiology. On the basis of the favorable outcome of the first NHP PET imaging studies, [^{18}F]3 has been investigated for detailed quantitative analysis and a target occupancy study in NHPs. It has also been advanced to test-retest and dosimetry studies in humans. The results from these studies will be communicated in future publications.

EXPERIMENTAL PROCEDURES

Biology. The sAPP β whole-cell assay, BACE1 enzyme cell-free assay, BACE2 enzyme cell-free assay, and cathepsin D enzyme cell-free assay were performed following the protocols that were previously described.²⁸

Pharmacokinetics. NeuroPK study in male CD-1 mice was carried out following the same protocol described in ref 17. The unbound fraction in mixed gender mouse (CD-1) plasma (Fu_p) was determined using the Rapid Equilibrium Device (RED, Thermo Scientific). A spiked mice plasma (2 μM) sample was prepared and added (220 μL) to the donor side, followed by addition of buffer (350 μL) to the receiver side. The RED device was then incubated at 37 $^\circ\text{C}$ for 4 h. Following the incubation, plasma (15 μL) and buffer (45 μL) were sampled and mixed with the appropriate blank matrix to prepare mixed matrix samples. Samples were protein precipitated with acetonitrile containing internal standard (200 μL), vortexed, and centrifuged. Supernatants were analyzed using an LC-MS/MS assay.

The buffer dilution factor was 0.33 (15 μL /45 μL). Fu_p was then calculated using (concentration in buffer sample \times 0.33)/(concentration in plasma sample). The unbound fraction in brain tissue homogenate (Fu_b) was determined using the 96-well equilibrium dialysis method described by Kalvass et al.²⁹ with the following exceptions. Brain homogenates were prepared from freshly harvested rat whole brains (Wistar han) following dilution with a 10-fold volume of phosphate buffer and spiked with 2 μM test compound. The homogenates were dialyzed against an equal volume (150 μL) of phosphate buffer at 37 $^\circ\text{C}$ for 6 h. Following the incubation, equal volumes (50 μL) of brain homogenate and buffer samples were collected and mixed with 50 μL of buffer or control homogenate, respectively, for preparation of mixed matrix samples. All samples were then precipitated with internal standard in acetonitrile (200 μL), vortexed, and centrifuged. Supernatants were analyzed using an LC-MS/MS assay. A dilution factor of 10 was applied to the calculation of brain fraction unbound.

Saturation Binding. The saturation binding of [^3H]1 in mouse brain tissue was performed using filtration separation of ligand bound in crude tissue homogenate. The source of tissue was frontal cortex from wild-type, heterozygous, and homozygous BACE1 KO mice. The [^3H]1 was titrated from 0.1 to 10 nM and incubated for 60 min at rt with 2.4 mg of tissue homogenate (homogenized at 12 mg/mL on ice for 8 s using polytron setting 5) in 250 μL of 50 mM Tris, pH 7.4, containing 2 mM MgCl_2 . Following incubation, samples were separated over GF/B filters that were presoaked in 0.1% polyethyleneimine followed by three washes with cold assay buffer. The amount of specific binding was calculated as the counts bound in the presence of 0.1% DMSO vehicle minus the counts bound in the presence of excess BACE1 inhibitor (10 μM).

Chemistry. General Methods. All solvents and reagents were of reagent grade and were used as supplied by the manufacturer. All reactions were run under a N_2 atmosphere. Organic extracts were routinely dried over anhydrous Na_2SO_4 or MgSO_4 . Concentration in vacuo refers to rotary evaporation under reduced pressure. Chromatography refers to flash chromatography using disposable RediSepRf 4 to 120 g silica columns or Biotage disposable columns on a CombiFlash Companion or Biotage Horizon automatic purification system. Purification by mass-triggered HPLC was carried out using Waters XTerra PrepMS C18 columns, 5 μm , 30 mm \times 100 mm. Compounds were presalted as TFA salts and diluted with 1 mL of DMSO. Samples were purified by mass-triggered collection using a mobile phase of acetonitrile and 0.1% TFA in water, with a gradient of 100% aqueous to 100% acetonitrile over 10 min at a flow rate of 20 mL/min. All target compounds were analyzed using ultra high performance liquid chromatography/ultraviolet/evaporative light scattering detection coupled to time-of-flight mass spectrometry (UHPLC/UV/ELSD/TOFMS). LC-MS analyses were performed on a Waters Acquity UPLC-MS system with a Waters Acquity HSS T3, 1.7 μm C18 column (50 mm \times 2.1 mm). UPLC conditions: mobile phase A = 0.1% formic acid in water (v/v), mobile phase B = 0.1% formic acid in acetonitrile; flow rate = 1.25 mL/min; compounds were eluted with a gradient of 5% B/A to 95% B/A for 1.1 min. All tested compounds were found to be >95% pure by this method.

N-(3-((4*a*S,5*S*,7*a*S)-2-Amino-5-(fluoromethyl)-4*a*,5-dihydro-4*H*-furo[3,4-*d*][1,3]thiazin-7*a*(7*H*)-yl)-4-fluorophenyl)-5-methoxypyrazine-2-carboxamide (3). To a stirring mixture of 11 (360 mg, 0.667 mmol) in anhydrous MeOH (6.5 mL) was added DBU (71.3 mg, 0.468 mmol, 0.070 mL) at rt. The reaction mixture was stirred at 60 $^\circ\text{C}$ for 6 h, during which time a white solid formed. The reaction was stirred at 60 $^\circ\text{C}$ for an additional 2.5 h then at rt overnight. The resulted white solid was collected by filtration, rinsed with cold MeOH (3 mL), and then dried in vacuo to afford 3 (224 mg, 77% yield) as a white solid. HRMS: calculated for $\text{C}_{19}\text{H}_{20}\text{F}_2\text{N}_5\text{O}_3\text{S}$ [$\text{M} + \text{H}$] $^+$ 436.1249, found 436.1256. Anal. Calcd for $\text{C}_{19}\text{H}_{19}\text{F}_2\text{N}_5\text{O}_3\text{S}$: C, 52.41; H, 4.40; N, 16.08. Found: C, 52.16; H, 4.35; N, 15.93. [α] $_\text{D}^{23.0} = +121.9^\circ$ (c 0.36, CHCl_3). ^1H NMR (400 MHz, $\text{DMSO}-d_6$) δ 10.56 (s, 1H), 8.89 (d, $J = 1.3$ Hz, 1H), 8.40 (d, $J = 1.3$ Hz, 1H), 7.89 (dd, $J = 7.3, 2.6$ Hz, 1H), 7.84 (ddd, $J = 8.6, 4.0, 2.8$ Hz, 1H), 7.15 (dd, $J = 11.9, 8.8$ Hz, 1H), 6.03 (s, 2H), 4.68–4.43 (m, 2H), 4.34 (dddd, J

= 23.5, 7.7, 5.1, 2.4 Hz, 1H), 4.24 (d, J = 8.2 Hz, 1H), 4.02 (s, 3H), 3.79 (dd, J = 8.1, 3.2 Hz, 1H), 3.13 (dd, J = 13.5, 3.6 Hz, 1H), 3.00 (dd, J = 13.5, 3.8 Hz, 1H), 2.75 (dt, J = 7.8, 3.7, 3.7 Hz, 1H). ^{13}C NMR (101 MHz, DMSO- d_6) δ 161.63, 161.45, 155.99 (d, J = 243.6 Hz), 148.36, 141.53, 137.92, 134.37 (d, J = 2.3 Hz), 133.53, 130.14 (d, J = 12.4 Hz), 122.12 (d, J = 4.1 Hz), 120.91 (d, J = 8.4 Hz), 116.16 (d, J = 25.0 Hz), 83.56 (d, J = 169.7 Hz), 78.52 (d, J = 18.2 Hz), 77.53 (d, J = 6.1 Hz), 65.80–65.36 (m), 54.29, 35.51 (dd, J = 5.1, 2.4 Hz), 22.97.

tert-Butyl ((4*a*R,8*a*S)-8*a*-(2-Fluoro-5-(5-hydroxypyrazine-2-carboxamido)phenyl)-4*a*,5,6,8*a*-hexahydropyrano[3,4-*d*][1,3]-thiazin-2-yl)carbamate (5). To a stirring solution of 5-hydroxypyrazine-2-carboxylic acid (74.7 mg, 0.53 mmol) in DMF (2 mL) were added DIPEA (116 μL , 0.67 mmol), HBTU (230 mg, 0.58 mmol), and **4**¹¹ (170 mg, 0.45 mmol) in that order. The reaction was flushed with nitrogen and stirred at rt for 3 h. The reaction was diluted with EtOAc and saturated aqueous NaHCO_3 solution and extracted. The organic extract was washed with water and brine then dried over Na_2SO_4 and concentrated to afford the crude product. Purification via flash column chromatography (silica gel, gradient 50% \rightarrow 100% EtOAc in heptanes) afforded **5** (76 mg, 34%) as an off-white solid. LC-MS m/z 504.3 $[\text{M} + \text{H}]^+$. ^1H NMR (400 MHz, CD_3OD) δ 8.13 (d, J = 1.3 Hz, 1H), 8.08 (d, J = 1.3 Hz, 1H), 7.84 (ddd, J = 2.7, 4.2, 8.8 Hz, 1H), 7.68 (dd, J = 2.6, 7.1 Hz, 1H), 7.18 (dd, J = 8.9, 12.2 Hz, 1H), 4.07 (td, J = 3.9, 11.3, 11.9 Hz, 2H), 3.78 (d, J = 11.8 Hz, 1H), 3.70 (td, J = 2.2, 12.2, 12.2 Hz, 1H), 3.14–3.07 (m, 1H), 2.98 (dd, J = 3.8, 13.0 Hz, 1H), 2.74 (dd, J = 3.0, 12.9 Hz, 1H), 2.15–2.03 (m, 1H), 1.62 (ddt, J = 1.6, 1.6, 3.3, 13.0 Hz, 1H), 1.52 (s, 9H).

((4*a*S,5*S*,7*a*S)-2-Benzamido-7*a*-(5-bromo-2-fluorophenyl)-4*a*,5,7,7*a*-tetrahydro-4*H*-furo[3,4-*d*][1,3]thiazin-2-yl)methyl formate (7). A mixture of **6**¹⁹ (10.0 g, 14.131 mmol) in formic acid (70 mL) was stirred at rt overnight. LC/MS showed **6** was consumed completely and the major peak was the desired formate ester. The solid was removed by filtration and the filtrate was washed with petroleum ether (75 mL \times 3). The formic acid layer was concentrated to give crude **7** (7.00 g) as yellow oil, which was carried directly into the next reaction.

***N*-((4*a*S,5*S*,7*a*S)-7*a*-(5-Bromo-2-fluorophenyl)-5-(hydroxymethyl)-4*a*,5,7,7*a*-tetrahydro-4*H*-furo[3,4-*d*][1,3]thiazin-2-yl)benzamide (8).** A mixture of the crude formate ester **7** (7.00 g, 14.19 mmol) and LiOH (1.70 g, 70.9 mmol) in THF/ H_2O (100 mL, 1/1 v/v) was stirred at rt for 1 h. LC/MS showed the reaction was complete. The organic layer was removed in vacuo, and water (50 mL) was added. The mixture was extracted with DCM (150 mL \times 3). The organic layer was washed with brine solution (100 mL), dried, filtered, and concentrated to afford crude **8** (5.60 g) as a light-yellow solid, which was carried directly into the next reaction without further purification.

***N*-((4*a*S,5*S*,7*a*S)-7*a*-(5-Bromo-2-fluorophenyl)-5-(fluoromethyl)-4*a*,5,7,7*a*-tetrahydro-4*H*-furo[3,4-*d*][1,3]thiazin-2-yl)benzamide (9).** To a stirred solution of the crude primary alcohol **8** (5.60 g, 12.03 mmol) in dry THF (150 mL) was added triethylamine (12.2 g, 120 mmol), triethylamine trihydrofluoride (6.6 g, 40.9 mmol), and perfluorobutane sulfonyl fluoride (12.4 g, 40.9 mmol) in that order at 0 $^\circ\text{C}$ under nitrogen. After addition, the mixture was stirred at 30–40 $^\circ\text{C}$ for 3 h. TLC (petroleum ether:EtOAc = 3:1) showed the reaction was complete. The mixture was poured into ice–water (200 mL), saturated aqueous NaHCO_3 (200 mL) was added, and the mixture was extracted with EtOAc (200 mL \times 2). The organic layer was washed with brine solution (150 mL \times 2), dried over Na_2SO_4 , filtered, and concentrated to give a residue, which was purified by flash column chromatography (silica gel; gradient 0% \rightarrow 30% EtOAc in petroleum ether) to afford **9** (3.40 g, 60.5%) as a white solid. LC-MS m/z 468.7 $[\text{M} + \text{H}]^+$. ^1H NMR (400 MHz, CDCl_3) δ 8.13–7.99 (m, 2H), 7.60–7.41 (m, 5H), 7.03 (dd, J = 8.7, 11.7 Hz, 1H), 4.73–4.53 (m, 3H), 4.52–4.46 (m, 1H), 4.03–3.95 (m, 1H), 3.36–3.28 (m, 1H), 3.27–3.17 (m, 1H), 2.85–2.76 (m, 1H).

***N*-((4*a*S,5*S*,7*a*S)-7*a*-(5-Amino-2-fluorophenyl)-5-(fluoromethyl)-4*a*,5,7,7*a*-tetrahydro-4*H*-furo[3,4-*d*][1,3]thiazin-2-yl)benzamide (10).** To a solution of **9** (865 mg, 1.81 mmol) in absolute EtOH (35 mL) was added N,N' -dimethylcyclohexane-1,2-diamine (300 mg, 2.11 mmol), followed by addition of sodium azide (1.20 g, 18.46 mmol)

and a solution of sodium L-ascorbate (185 mg, 0.93 mmol) in water (10 mL) at rt. The mixture was stirred under nitrogen for 15 min, then copper(I) iodide (175 mg, 0.92 mmol) was added and the mixture was heated at 70 $^\circ\text{C}$ for 2 h. LC/MS showed the reaction was complete. The mixture was concentrated in vacuo then partitioned between brine solution (50 mL) and EtOAc (100 mL). The phases were separated, and the aqueous layer was extracted three times with additional EtOAc. The combined organic layers were dried over Na_2SO_4 , filtered, and concentrated to give crude product which was purified by flash column chromatography (silica gel, gradient 0% \rightarrow 100% EtOAc in heptanes) to afford **10** (524 mg, 72%) as a white solid. LC-MS m/z 404.1 $[\text{M} + \text{H}]^+$. ^1H NMR (400 MHz, CDCl_3) δ 12.03 (s, 1H), 8.17 (d, J = 7.1 Hz, 2H), 7.56–7.50 (m, 1H), 7.45 (t, J = 7.5, 7.5 Hz, 2H), 6.92 (dd, J = 8.7, 11.9 Hz, 1H), 6.70 (dd, J = 2.6, 6.5 Hz, 1H), 6.61 (dt, J = 3.3, 3.3, 8.5 Hz, 1H), 4.74–4.49 (m, 4H), 4.08–3.98 (m, 1H), 3.69 (s, 2H), 3.46–3.38 (m, 1H), 3.29 (dd, J = 3.4, 13.8 Hz, 1H), 2.81 (dd, J = 3.6, 13.8 Hz, 1H).

***N*-((4*a*S,5*S*,7*a*S)-2-Benzamido-5-(fluoromethyl)-4*a*,5-dihydro-4*H*-furo[3,4-*d*][1,3]thiazin-7*a*(7*H*)-yl)-4-fluorophenyl)-5-methoxypyrazine-2-carboxamide (11).** To a solution of 5-methoxypyrazine-2-carboxylic acid (120 mg, 0.78 mmol) and **10** (300 mg, 0.74 mmol) in acetonitrile (10 mL) was added DIPEA (300 μL , 1.72 mmol) followed by HATU (300 mg, 0.79 mmol) at rt. The mixture was stirred at rt for 30 min. LC-MS showed the reaction was completed. The mixture was concentrated in vacuo, diluted with EtOAc (40 mL), then washed with water (15 mL) and brine solution (15 mL). The organic extract was dried over Na_2SO_4 filtered and concentrated to give crude product, which was purified by flash column chromatography (24 g silica gel, gradient 0% \rightarrow 100% EtOAc in heptanes) to afford compound **11** (374 mg, 93%) as a white solid. LC-MS m/z 540.1 $[\text{M} + \text{H}]^+$. ^1H NMR (400 MHz, CDCl_3) δ 12.66 (s, 1H), 9.56 (s, 1H), 9.00 (s, 1H), 8.25–8.05 (m, 3H), 7.91 (d, J = 7.7 Hz, 1H), 7.72–7.64 (m, 1H), 7.57–7.50 (m, 1H), 7.46 (t, J = 7.3, 7.3 Hz, 2H), 7.18 (dd, J = 8.9, 11.5 Hz, 1H), 4.76–4.54 (m, 3H), 4.51 (d, J = 9.3 Hz, 1H), 4.12 (q, J = 7.1, 7.1, 7.1 Hz, 1H), 4.06 (s, 3H), 3.50–3.32 (m, 2H), 2.94–2.81 (m, 1H).

***N*-((4*a*S,5*S*,7*a*S)-7*a*-(5-Amino-2-fluorophenyl)-5-((trityloxy)methyl)-4*a*,5,7,7*a*-tetrahydro-4*H*-furo[3,4-*d*][1,3]thiazin-2-yl)benzamide (12).** To a solution of compound **6**¹⁹ (7.08 g, 10.00 mmol) in EtOH (210 mL) was added N,N' -dimethylcyclohexane-1,2-diamine (1.71 g, 12.0 mmol), followed by addition of solid sodium azide (6.18 g, 95.06 mmol) and a solution of sodium L-ascorbate (931 mg, 4.70 mmol) in water (60 mL) at rt under a nitrogen atmosphere. Then copper(I) iodide (895 mg, 4.70 mmol) was added, and the mixture was heated at 70 $^\circ\text{C}$ for 2 h. The mixture was diluted with water (300 mL) and EtOAc (200 mL) and extracted with additional EtOAc (100 mL \times 2). The combined organic layers were washed with brine solution (200 mL), dried over Na_2SO_4 , filtered, and concentrated to give crude aniline **12** (6.44g, 72% purity) as yellow oil, which was used directly in the next step without further purification. LC-MS m/z 666.1 $[\text{M} + \text{Na}]^+$.

***N*-((4*a*S,5*S*,7*a*S)-2-Benzamido-5-((trityloxy)methyl)-4*a*,5-dihydro-4*H*-furo[3,4-*d*][1,3]thiazin-7*a*(7*H*)-yl)-4-fluorophenyl)-5-methoxypyrazine-2-carboxamide (13).** To a mixture of the aniline **12** (6.44 g, \sim 72% purity, 7.2 mmol) and commercially available 5-methoxypyrazine-2-carboxylic acid (1.33 g, 8.64 mmol) in DCM (100 mL) was added pyridine (2.28 g, 28.8 mmol) at rt, followed by addition of a solution of propylphosphonic anhydride solution (aka T3P, 50% by wt. in EtOAc, 13.8 g, 21.6 mmol) dropwise at rt and stirred at that temperature for 16 h. The mixture was quenched with water (200 mL) and extracted with DCM (2 \times 100 mL). The combined organic layers were washed with brine solution (300 mL), dried, and concentrated to give crude product, which was purified by flash column chromatography on silica gel (40 g silica gel, 0% \rightarrow 15% EtOAc in petroleum ether) to afford **13** (2.3 g, 41% over two steps) as a yellow semisolid. LC-MS m/z 780.2 $[\text{M} + \text{H}]^+$. ^1H NMR (400 MHz, CDCl_3) δ 9.54 (s, 1H), 9.00 (s, 1H), 8.20–8.14 (m, 2H), 8.13 (s, 1H), 8.01–7.95 (m, 1H), 7.56 (d, J = 5.2 Hz, 1H), 7.53–7.50 (m, 1H), 7.49–7.42 (m, 7H), 7.35–7.29 (m, 5H), 7.28–7.21 (m, 5H), 7.16 (dd, J = 9.2, 11.7 Hz, 1H), 4.62–4.52 (m, 2H), 4.12–4.09 (m, 1H), 4.06 (s,

3H), 3.48–3.42 (m, 1H), 3.41–3.31 (m, 2H), 3.28–3.21 (m, 1H), 2.71 (dd, $J = 3.4, 13.9$ Hz, 1H).

((4*aS*,5*S*,7*aS*)-2-Benzamido-7*a*-(2-fluoro-5-(5-methoxypyrazine-2-carboxamido)phenyl)-4*a*,5,7,7*a*-tetrahydro-4*H*-furo[3,4-*d*][1,3]-thiazin-5-yl)methyl formate (**14**). Formic acid (30 mL) was added to **13** (2.30 g, 2.95 mmol) neat at 0 °C. After the addition, the mixture was warmed to rt and stirred at ambient temperature for 16 h. TLC (petroleum ether/EtOAc = 3/1) showed the reaction was complete. The mixture was concentrated in vacuo to give the corresponding formate ester **14** (1.67 g, crude, quant) as a yellow solid, which was used directly in the next step.

N-(3-((4*aS*,5*S*,7*aS*)-2-Benzamido-5-(hydroxymethyl)-4*a*,5-dihydro-4*H*-furo[3,4-*d*][1,3]thiazin-7*a*(7*H*)-yl)-4-fluorophenyl)-5-methoxypyrazine-2-carboxamide (**15**). To a solution of crude formate ester **14** (1.67 g, 2.95 mmol) in THF/water (40 mL, 1/1 v/v) was added LiOH (141 mg, 5.91 mmol) at rt and stirred at the same temperature for 20 min. TLC (pet ether/EtOAc = 1:1, UV) showed the reaction was complete. The reaction was diluted with water (100 mL) and extracted with EtOAc (30 mL × 2). The organic layer was washed with brine solution (50 mL × 2), dried over Na₂SO₄, filtered, and concentrated afford compound **15** (1.59 g, quant. over two steps) as a yellow semisolid. LC-MS m/z 538.0 [M + H]⁺. ¹H NMR (400 MHz, CDCl₃) δ 9.55 (s, 1H), 8.99 (s, 1H), 8.20–8.10 (m, 3H), 7.91–7.84 (m, 1H), 7.71–7.65 (m, 1H), 7.54–7.49 (m, 1H), 7.48–7.41 (m, 2H), 7.16 (dd, $J = 8.8, 11.7$ Hz, 1H), 4.57–4.52 (m, 1H), 4.50 (d, $J = 9.6$ Hz, 1H), 4.18–4.11 (m, 1H), 4.06 (s, 3H), 3.96 (dd, $J = 2.6, 11.8$ Hz, 1H), 3.75 (dd, $J = 3.5, 11.5$ Hz, 1H), 3.44–3.33 (m, 2H), 2.87 (dd, $J = 2.1, 14.1$ Hz, 1H), 2.04 (s, 1H).

N-(3-((4*aS*,5*S*,7*aS*)-2-Amino-5-(hydroxymethyl)-4*a*,5-dihydro-4*H*-furo[3,4-*d*][1,3]thiazin-7*a*(7*H*)-yl)-4-fluorophenyl)-5-methoxypyrazine-2-carboxamide (**16**). To a solution of compound **15** (700 mg, 1.30 mmol) in MeOH (25 mL) was added DBU (1.98 g, 13.0 mmol) at rt. The reaction mixture was stirred at 60 °C for 3 h, during which time a white solid formed and LC/MS showed the reaction was complete. The reaction was filtered, and the white solid was dried to afford crude compound **16** (500 mg, 80% purity by LC-MS), which was advanced as-is into the next step. LC-MS m/z 456.0 [M + Na]⁺.

tert-Butyl ((4*aS*,5*S*,7*aS*)-7*a*-(2-Fluoro-5-(5-methoxypyrazine-2-carboxamido)phenyl)-5-(hydroxymethyl)-4*a*,5,7,7*a*-tetrahydro-4*H*-furo[3,4-*d*][1,3]thiazin-2-yl)carbamate (**17**). To a suspension of compound **16** (500 mg, 1.15 mmol) in tetrahydrofuran (200 mL) was added Boc₂O (378 mg, 1.73 mmol) and triethylamine (233 mg, 2.31 mmol) at rt. The suspension was stirred at 60 °C for 16 h. The mixture was concentrated to afford the crude product (0.95 g), which was subjected to flash column chromatography (4 g silica gel, 0% → 5% in DCM) followed by repurification via preparative HPLC (Column, Agella Durashell C18 250 mm × 21.2 mm 5 μm particle size; mobile phase, from 36% → 56% acetonitrile in aqueous ammonia (pH 10) to 56% acetonitrile in ammonia). The pure preparative HPLC fractions were concentrated and lyophilized to afford compound **17** (400 mg, 58% over 2 steps) as a white solid. LC-MS m/z 556.1 [M + Na]⁺. ¹H NMR (400 MHz, CDCl₃) δ 9.53 (s, 1H), 9.01 (d, $J = 1.3$ Hz, 1H), 8.18 (d, $J = 1.3$ Hz, 1H), 7.97–7.89 (m, 1H), 7.56–7.41 (m, 1H), 7.11 (dd, $J = 8.9, 11.6$ Hz, 1H), 4.50 (d, $J = 9.0$ Hz, 1H), 4.48–4.44 (m, 1H), 4.07 (s, 3H), 3.99–3.85 (m, 2H), 3.76–3.68 (m, 1H), 3.27–3.05 (m, 2H), 2.74 (dd, $J = 2.7, 12.6$ Hz, 1H), 2.14 (s, 1H), 1.52 (s, 9H).

((4*aS*,5*S*,7*aS*)-2-((*tert*-Butoxycarbonyl)amino)-7*a*-(2-fluoro-5-(5-methoxypyrazine-2-carboxamido)phenyl)-4*a*,5,7,7*a*-tetrahydro-4*H*-furo[3,4-*d*][1,3]thiazin-5-yl)methyl 4-methylbenzenesulfonate (**18**). To a stirred solution of **17** (135 mg, 0.325 mmol) in DCM (1.1 mL) were added tosyl chloride (160 mg, 0.839 mmol), DIPEA (111 mg, 0.861 mmol, 0.150 mL), and DMAP (11 mg, 0.09 mmol) in that order. The reaction was stirred at rt for 20 h. The reaction was diluted with DCM (10 mL) then washed sequentially with 0.25 N aqueous HCl (3 mL), water (2 mL), saturated aqueous NaHCO₃ solution (1 mL), and brine solution (1 mL). The organic extract was dried over Na₂SO₄, filtered, and concentrated to afford a crude product. Purification via flash column chromatography (silica gel, gradient 0 → 100% EtOAc in heptanes) to afford a white solid (123 mg), which was further purified by flash column chromatography

(silica gel, gradient 5 → 20% acetonitrile in DCM) to afford **18** (98 mg, 56% yield) as a white solid. HRMS: calculated for C₃₁H₃₅FN₅O₈S₂ [M + H]⁺ 688.1906, found 688.1907. Anal. Calcd for C₃₁H₃₄FN₅O₈S₂: C, 54.14; H, 4.98; N, 10.18. Found: C, 53.88; H, 4.94; N, 9.85. [α]_D^{23.1} = +67.8° (c 0.345, CHCl₃). ¹H NMR (400 MHz, acetonitrile-*d*₃) δ 9.67 (s, 1H), 8.91 (s, 1H), 8.35 (s, 1H), 8.22 (d, $J = 1.3$ Hz, 1H), 7.88 (ddd, $J = 8.8, 4.1, 2.8$ Hz, 1H), 7.79 (d, $J = 8.3$ Hz, 2H), 7.62 (dd, $J = 7.1, 2.6$ Hz, 1H), 7.42 (d, $J = 8.0$ Hz, 2H), 7.12 (dd, $J = 12.0, 8.9$ Hz, 1H), 4.37 (ddd, $J = 8.2, 5.2, 3.6$ Hz, 1H), 4.31 (d, $J = 8.9$ Hz, 1H), 4.25–4.12 (m, 2H), 4.03 (s, 3H), 3.74 (dd, $J = 8.7, 2.5$ Hz, 1H), 3.00–2.91 (m, 1H), 2.91–2.84 (m, 1H), 2.72–2.62 (m, 1H), 2.42 (s, 3H), 1.46 (s, 9H). ¹³C NMR (101 MHz, acetonitrile-*d*₃) δ 163.38, 162.46, 157.06 (d, $J = 243.5$ Hz), 146.54, 142.54, 138.46, 135.52 (d, $J = 2.5$ Hz), 134.63, 133.64, 131.03, 128.92 (d, $J = 11.5$ Hz), 128.81, 122.85 (m, br), 122.15 (d, $J = 8.7$ Hz), 117.65 (d, $J = 25.0$ Hz), 81.55, 78.31, 77.55 (d, $J = 6.5$ Hz), 71.40, 67.29 (d, $J = 5.1$ Hz), 55.12, 40.18 (d, $J = 3.1$ Hz), 28.35, 23.64, 21.67.

Radiosynthesis of [³H]1. A stirred solution of [³H]methyl iodide (1 Ci, 80 Ci/mmol, 12.5 μmol) in 0.5 mL of CHCl₃ was placed under N₂, cooled in an ice bath, and treated with a suspension of **5** (6.3 mg, 12.5 μmol, 1.0 equiv) in 0.5 mL of CHCl₃ and solid Ag₂CO₃ (3.5 mg, 12.7 μmol, 1.0 equiv). The reaction mixture was then warmed to rt and stirred for 30 h. The reaction mixture was filtered, and the solvent was removed in vacuo. The residue was then treated with 1 mL of trifluoroacetic acid, and the resulting solution was stirred at rt for 2 h. The reaction was then concentrated, and the residue was dissolved in 4 mL of EtOAc and washed with 4 mL of saturated aqueous solution of NaHCO₃. The organic layer was concentrated, and the residue was purified by reverse phase HPLC to yield 20 mCi of [³H]**1** with specific activity of 80 Ci/mmol and radiochemical purity >99%. The HPLC condition is as follows: Column, Zorbax SB-C18, 5 μm, 4.6 mm × 250 mm; column temperature, ambient; mobile phase A, 0.1% formic acid in H₂O; mobile phase B, acetonitrile; gradient, 10–100% B in 30 min; flow rate, 1 mL/min; run time, 30 min; detection, 254 nm.

LC-MS/MS Cold Tracer Method. Brain binding of compounds **2** and **3** in mice were evaluated with a LC-MS/MS based “cold tracer” assay. A total of three studies were performed. All procedures in this study were in compliance with the U.S. Department of Agriculture’s (USDA) Animal Welfare Act (9 CFR Parts 1, 2, and 3); the Guide for the Care and Use of Laboratory Animals: Eighth Edition, (Institute for Laboratory Animal Research, The National Academies Press, Washington, DC, 2010); and the National Institutes of Health, Office of Laboratory Animal Welfare. Whenever possible, procedures in this study were designed to avoid or minimize discomfort, distress, and pain to animals. In study 1, male CD-1 mice (25–35 g) were dosed with 100 mg/kg of BACE1 inhibitor A²² (100 mg/kg, SC) or vehicle ($n = 5$ per treatment group), followed by intravenous administration of the tracer, compound **2**, at 10 μg/kg dose 60 min post blocking compound or vehicle dosing. Mice were euthanized by live decapitation at 45 min post the tracer administration, and four brain tissues (cerebellum, frontal cortex, hippocampus and striatum) were dissected and the plasma samples were collected to measure the tracer concentration using LC-MS/MS.

In study 2, male 129/sve mice (20–25 g) were dosed with varying doses of BACE1 inhibitor B²³ (1, 10, or 80 mg/kg, SC) or vehicle ($n = 5$ per treatment group), followed by intravenous administration of the tracer, compound **3**, at 10 μg/kg dose 60 min inhibitor or vehicle dosing. Mice were then euthanized by live decapitation at 45 min post the tracer administration. The same four brain tissues plus plasma samples used in study 1 were collected to measure the tracer concentration.

In study 3, BACE1 KO and WT mice ($n = 5$ per group) were evaluated following the same procedure used in previous two studies, with the exception that no blocking compound was dosed.

PET Radiochemistry. No-carrier-added [¹⁸F]fluoride was produced from a GEMS PET trace Cyclotron using 16.4 MeV protons via the ¹⁸O(p,n)¹⁸F reaction on ¹⁸O enriched water ([¹⁸O]H₂O). [¹⁸F]Fluoride was isolated from [¹⁸O]H₂O on a preconditioned SepPak QMA light anion exchange cartridge and subsequently eluted from the cartridge with a solution of K₂CO₃ (1.8 mg, 13 μmol),

Kryptofix 2.2.2 (4,7,13,16,21,24-hexaoxa-1,10-diazabicyclo- [8.8.8]-hexacosane-K2.2.2) (9.8 mg, 26 μ mol) in water (85 μ L, 18 M Ω) and CH₃CN (2 mL) to a reaction vessel (10 mL). The solvents were evaporated at 160 °C for 10–12 min under continuous nitrogen flow (70 mL/min) to form a dry complex of [¹⁸F]fluoride/K2.2.2, and the residue was cooled to rt. The precursor **18** (~0.007 mmol, ~5 mg) in DMSO (600 μ L) was added to the dry complex of [¹⁸F]fluoride/K2.2.2. The closed reaction vessel was heated at 110 °C for 10 min and cooled down to rt. Removal of the Boc protecting group was carried out by adding aqueous HCl (2.0 N, 200 μ L) to the reaction mixture and heated at 100 °C for 5 min. The reaction mixture was cooled to rt and was diluted with water to a total volume of 2.0 mL before injecting to HPLC for purification. A radioactive fraction corresponding to [¹⁸F]**3** (retention time = 15–17 min) was collected and diluted with sterile water (50 mL). The resulting mixture was loaded onto a preconditioned SepPak tC18 plus cartridge. The cartridge was washed with water (10 mL), and the desired product [¹⁸F]**3** was eluted with EtOH (1 mL) into a sterile vial containing phosphate buffer saline solution (PBS, 9 mL). [¹⁸F]**3** was successfully radiosynthesized in 80–95 min from end of beam ($n = 2$) in 4 and 7% radiochemical yield (>99% purity), 187 and 417 MBq of delivered radioactivity, and 84 and 175 GBq/ μ mol of specific radioactivity at the time of injection, respectively.

NHP PET Imaging. [¹⁸F]**3** was evaluated with PET imaging in one female cynomolgus monkey (body weight approximately 5500 g). The monkey was scanned twice with PET, one baseline scan, and one blocking scan with pretreatment of a BACE1 inhibitor LY2886721.²⁴ Approximately 2 months separated the baseline and blocking scans. The study was approved by the Animal Ethics Committee of the Swedish Animal Welfare Agency and was performed according to the “Guidelines for Planning, Conducting, And Documenting Experimental Research” (Dnr 4820/06-600) of Karolinska Institutet (KI).

The monkey was immobilized and transported from its housing facility to the KI PET center after intramuscular injection of ketamine hydrochloride (approximately 10 mg/kg). The anesthesia was maintained by the administration of a mixture of isoflurane (1.5–2.0%), oxygen, and medical air after endotracheal intubation at the KI PET center. For the blocking study, 5 mg/kg of LY2886721 in 0.5% methylcellulose with a dosing volume of 2 mL/kg, followed with 2 mL of tap water, was administered orally (via gavage) approximately 2 h before PET scanning. The monkey's head was immobilized with a fixation device, and its body temperature was maintained by a Bair Hugger model 505 (Arizant Healthcare, MN) and monitored with an esophageal thermometer. The ECG, heart rate, respiratory rate, and oxygen saturation of the monkey were continuously monitored throughout the experiment. The monkey's fluid balance was maintained by a continuous infusion of saline.

Dynamic PET scan of 3 h was conducted using a High Resolution Research Tomograph (HRRT) (Siemens Molecular Imaging) following iv injection of the radioligand [¹⁸F]**3**. A transmission scan of 6 min using a single ¹³⁷Cs source was performed before the radioligand injection. List-mode data were reconstructed using the ordinary Poisson 3D-ordered subset expectation maximization (OP-3D-OSEM) algorithm, with 10 iterations and 16 subsets including modeling of the point spread function.

■ ASSOCIATED CONTENT

■ Supporting Information

The Supporting Information is available free of charge on the ACS Publications website at DOI: 10.1021/acs.jmedchem.7b01769.

¹H and ¹³C NMR spectra for compound **3** and tosylate precursor **18** with peak assignments; selectivity profile of compound **3** in the CEREP selectivity panel; uptake and tissue distribution of compounds **2** and **3** (5–75 min survival interval) in male wild-type mice (PDF)
Molecular formula strings (CSV)

■ AUTHOR INFORMATION

Corresponding Author

*Phone: (617) 395-0640. E-mail: Lei.Zhang3@pfizer.com.

ORCID

Lei Zhang: 0000-0001-8118-1402

Brian T. O'Neill: 0000-0002-1928-4803

Notes

The authors declare no competing financial interest.

■ ACKNOWLEDGMENTS

We thank Pfizer ADME technology group for generating the in vitro PK data and developing the in silico RRCK, MDR1 BA/AB, and brain fractions unbound models; BioDuro Inc. for performing the neuroPK study; Covance Inc. for performing the LC-MS/MS cold tracer study; all members of the PET group at the Karolinska Institutet for their kind assistance during the PET imaging study; Yong Zhang, Aijia Yu, and Jinlong Wang and their teams at WUXI Apptec for synthesis and scale-up efforts.

■ ABBREVIATIONS USED

AD, Alzheimer's disease; A β , β -amyloid; BACE1, β -site amyloid precursor protein cleaving enzyme 1; B/P, brain to plasma ratio; B_{max}, the maximum concentration of target binding sites; CatD, cathepsin D; CPM, count per minute; CSF, cerebrospinal fluid; FP, fluorescence polarization; Fu_b, fraction unbound in brain; KO, knockout; MDCK, Mardin–Darby canine kidney; MPO, multiparameter optimization; NHP, nonhuman primate; P_{app}, apparent permeability coefficient; PET, positron emission tomography; P-gp, P-glycoprotein; RED, rapid equilibrium device; RRCK, Ralph–Russ canine kidney; SUV, standardized uptake values; WT, wild-type

■ REFERENCES

- (1) 2012 Alzheimer's Disease facts and figures; Alzheimer's Association: Washington DC, 2012; https://www.alz.org/downloads/facts_figures_2012.pdf.
- (2) (a) Cummings, J. L.; Morstorf, T.; Zhong, K. Alzheimer's disease drug-development pipeline: few candidates, frequent failures. *Alzheimer's Res. Ther.* **2014**, *6*, 37. (b) Schneider, L. S.; Mangialasche, F.; Andreasen, N.; Feldman, H.; Giacobini, E.; Jones, R.; Mantua, V.; Mecocci, P.; Pani, L.; Winblad, B.; Kivipelto, M. Clinical trials and late-stage drug development for Alzheimer's disease: an appraisal from 1984 to 2014. *J. Intern. Med.* **2014**, *275*, 251–283.
- (3) (a) Nordberg, A. PET imaging of amyloid in Alzheimer's disease. *Lancet Neurol.* **2004**, *3*, 519–527. (b) Landau, S. M.; Thomas, B. A.; Thurfjell, L.; Schmidt, M.; Margolin, R.; Mintun, M.; Pontecorvo, M.; Baker, S. L.; Jagust, W. J. Amyloid PET imaging in Alzheimer's disease: a comparison of three radiotracers. *Eur. J. Nucl. Med. Mol. Imaging* **2014**, *41*, 1398–1407.
- (4) (a) Okamura, N.; Harada, R.; Furumoto, S.; Arai, H.; Yanai, K.; Kudo, Y. Tau PET imaging in Alzheimer's disease. *Curr. Neurol. Neurosci. Rep.* **2014**, *14*, 500. (b) James, O. G.; Doraiswamy, P. M.; Borges-Neto, S. PET imaging of Tau pathology in Alzheimer's disease and tauopathies. *Front. Neurol.* **2015**, *6*, 38.
- (5) (a) Holsinger, R. M. D.; Mclean, C. A.; Beyreuther, K.; Masters, C. L.; Evin, G. Increased expression of the amyloid precursor β -secretase in Alzheimer's disease. *Ann. Neurol.* **2002**, *51*, 783–786. (b) Fukumoto, H.; Cheung, B. S.; Hyman, B. T.; Irizarry, M. C. β -Secretase protein and activity are increased in the neocortex in Alzheimer disease. *Arch. Neurol.* **2002**, *59*, 1381–1389. (c) Zhao, J.; Fu, Y.; Yasvoina, M.; Shao, P.; Hitt, B.; O'Connor, T.; Logan, S.; Maus, E.; Citron, M.; Berry, R.; Binder, L.; Vassar, R. β -Site amyloid

precursor protein cleaving enzyme 1 levels become elevated in neurons around amyloid plaques: implications for Alzheimer's disease pathogenesis. *J. Neurosci.* **2007**, *27*, 3639–3649.

(6) Sadleir, K. R.; Kandalepas, P. C.; Buggia-Prévo, V.; Nicholson, D. A.; Thinakaran, G.; Vassar, R. Presynaptic dystrophic neurites surrounding amyloid plaques are sites of microtubule disruption, BACE1 elevation, and increased A β generation in Alzheimer's disease. *Acta Neuropathol.* **2016**, *132*, 235–256.

(7) For representative review articles on BACE1 inhibitors, please see: (a) Larner, A. J. Secretases as therapeutic targets in Alzheimer's disease: patents 2000–2004. *Expert Opin. Ther. Pat.* **2004**, *14*, 1403–1420. (b) Probst, G.; Xu, Y. Z. Small-molecule BACE1 inhibitors: a patent literature review (2006–2011). *Expert Opin. Ther. Pat.* **2012**, *22*, 511–540. (c) Vassar, R. BACE1 inhibitor drugs in clinical trials for Alzheimer's disease. *Alzheimer's Res. Ther.* **2014**, *6*, 89. (d) Oehlrich, D.; Prokopcova, H.; Gijssen, H. J. M. The evolution of amidine-based brain penetrant BACE1 inhibitors. *Bioorg. Med. Chem. Lett.* **2014**, *24*, 2033–2045.

(8) Zhang, L.; Villalobos, A. Strategies to facilitate the discovery of novel CNS PET ligands. *EJNMMI Radiopharm. Chem.* **2017**, *1*, 13.

(9) Zhang, L.; Villalobos, A.; Beck, E. M.; Bocan, T.; Chappie, T. A.; Chen, L.; Grimwood, S.; Heck, S. D.; Helal, C. J.; Hou, X.; Humphrey, J. M.; Lu, J.; Skaddan, M. B.; McCarthy, T. J.; Verhoest, P. R.; Wager, T. T.; Zasadny, K. Design and selection parameters to accelerate the discovery of novel central nervous system positron emission tomography (PET) ligands and their application in the development of a novel phosphodiesterase 2A PET ligand. *J. Med. Chem.* **2013**, *56*, 4568–4579.

(10) (a) Chernet, E.; Martin, L. J.; Li, D.; Need, A. B.; Barth, V. N.; Rash, K. S.; Phebus, L. A. Use of LC/MS to assess brain tracer distribution in preclinical, in vivo receptor occupancy studies: Dopamine D2, serotonin 2A and NK-1 receptors as examples. *Life Sci.* **2005**, *78*, 340–346. For additional applications, please see. (b) Pike, V. W.; Rash, K. S.; Chen, Z.; Pedregal, C.; Statnick, M. A.; Kimura, Y.; Hong, J.; Zoghbi, S. S.; Fujita, M.; Toledo, M. A.; Diaz, N.; Gackenheim, S. L.; Tauscher, J. T.; Barth, V. N.; Innis, R. B. Synthesis and evaluation of radioligands for imaging brain nociceptin/orphanin FQ peptide (NOP) receptors with positron emission tomography. *J. Med. Chem.* **2011**, *54*, 2687–2700. (c) Mitch, C. H.; Quimby, S. J.; Diaz, N.; Pedregal, C.; de la Torre, M. G.; Jimenez, A.; Shi, Q.; Canada, E. J.; Kahl, S. D.; Statnick, M. A.; McKinzie, D. L.; Benesh, D. R.; Rash, K. S.; Barth, V. N. Discovery of amino-benzoyloxyarylamides as κ opioid receptor selective antagonists: Application to preclinical development of a κ opioid receptor antagonist receptor occupancy tracer. *J. Med. Chem.* **2011**, *54*, 8000–8012.

(11) Motoki, T.; Takeda, K.; Takaishi, M.; Suzuki, Y.; Ishida, T. Novel Fused Aminodihydrothiazine Derivatives. WO 2010038686A1, Apr 8, 2010.

(12) Yan, R.; Bienkowski, M. J.; Shuck, M. E.; Miao, H.; Tory, M. C.; Pauley, A. M.; Brashler, J. R.; Stratman, N. C.; Mathews, W. R.; Buhl, A. E.; Carter, D. B.; Tomasselli, A. G.; Parodi, L. A.; Heinrikson, R. L.; Gurney, M. E. Membrane-anchored aspartyl protease with Alzheimer's disease beta-secretase activity. *Nature* **1999**, *402*, 533–537.

(13) Bennett, B. D.; Babu-Khan, S.; Loeloff, R.; Louis, J. – C.; Curran, E.; Citron, M.; Vassar, R. Expression analysis of BACE2 in brain and peripheral tissues. *J. Biol. Chem.* **2000**, *275*, 20647–20651.

(14) Vassar, R.; Bennett, B. D.; Babu-Khan, S.; Kahn, S.; Mendiaz, E. A.; Denis, P.; Teplow, D. B.; Ross, S.; Amarante, P.; Loeloff, R.; Luo, Y.; Fisher, S.; Fuller, J.; Edenson, S.; Lile, J.; Jarosinski, M. A.; Biere, A. L.; Curran, E.; Burgess, T.; Louis, J.-C.; Collins, F.; Treanor, J.; Rogers, G.; Citron, M. β -Secretase cleavage of Alzheimer's amyloid precursor protein by the transmembrane aspartic protease BACE. *Science* **1999**, *286*, 735–741.

(15) Patel, S.; Gibson, R. In vivo site-directed radiotracers: a mini-review. *Nucl. Med. Biol.* **2008**, *35*, 805–815.

(16) Keefer, C. E.; Kauffman, G. W.; Gupta, R. R. Interpretable, probability-based confidence metric for continuous quantitative

structure-activity relationship models. *J. Chem. Inf. Model.* **2013**, *53*, 368–383.

(17) Brodney, M. A.; Beck, E. M.; Butler, C. R.; Barreiro, G.; Johnson, E. F.; Riddell, D.; Parris, K.; Nolan, C. E.; Fan, Y.; Atchison, K.; Gonzales, C.; Robshaw, Q. E.; Doran, S. D.; Bundesmann, M. W.; Buzon, L.; Dutra, J.; Henegar, K.; LaChapelle, E.; Hou, X.; Rogers, B. N.; Pandit, J.; Lira, R.; Martinez-Alsina, L.; Mikochik, P.; Murray, J. C.; Ogilvie, K.; Price, L.; Sakya, S. M.; Yu, A.; Zhang, Y.; O'Neill, B. T. Utilizing structures of CYP2D6 and BACE1 complexes to reduce risk of drug–drug interactions with a novel series of centrally efficacious BACE1 inhibitors. *J. Med. Chem.* **2015**, *58*, 3223–3252.

(18) Takaishi, M.; Ishida, T. Fused Aminohydrothiazine Derivatives. WO 2012098461A1, Jul 26, 2012.

(19) Lombardo, F.; Shalaeva, M. Y.; Tupper, K. A.; Gao, F. ElogD_{0.1}: A tool for lipophilicity determination in drug discovery. 2. Basic and neural compounds. *J. Med. Chem.* **2001**, *44*, 2490–2497.

(20) Fu_b was measured using rat brain homogenate based on species independence in brain tissue bindings. For a reference, please see: Di, L.; Umland, J. P.; Chang, G.; Huang, Y.; Lin, Z.; Scott, D. O.; Troutman, M. D.; Liston, T. E. Species independence in brain tissue binding using brain homogenates. *Drug Metab. Dispos.* **2011**, *39*, 1270–1277.

(21) Remick, D. M.; Richards, S. J.; Sanderson, A. J. Tetrahydrofuran-fused Aminohydrothiazine Derivatives Which are Useful in the Treatment of Alzheimer's Disease. WO 2016176118A1, Nov 3, 2016.

(22) Richards, S. J.; Hembre, E. J.; Lopez, J. E.; Winneroski, L. L., Jr.; Woods, T. A.; McMahon, J. A. Selective BACE1 Inhibitors. US 20160244465AA, Aug 25, 2016.

(23) Goriya, Y.; Ramana, C. V. The [Cu]-catalyzed S_NAr reactions: direct amination of electron deficient aryl halides with sodium azide and the synthesis of arylthioethers under Cu (II)-ascorbate redox system. *Tetrahedron* **2010**, *66*, 7642–7650.

(24) Compound 36 in Butler, C. R.; Brodney, M. A.; Beck, E. M.; Barreiro, G.; Nolan, C. E.; Pan, F.; Vajdos, F.; Parris, K.; Varghese, A. H.; Helal, C. J.; Lira, R.; Doran, S. D.; Riddell, D. R.; Buzon, L. M.; Dutra, J. K.; Martinez-Alsina, L. A.; Ogilvie, K.; Murray, J. C.; Young, J. M.; Atchison, K.; Robshaw, A.; Gonzales, C.; Wang, J.; Zhang, Y.; O'Neill, B. T. Discovery of a series of efficient, centrally efficacious BACE1 inhibitors through structure-based drug design. *J. Med. Chem.* **2015**, *58*, 2678–2702.

(25) Brodney, M. A.; Beck, E. M.; Butler, C. R.; Zhang, L.; O'Neill, B. T.; Barreiro, G.; Lachapelle, E. A.; Rogers, B. N. Preparation of *N*-(2-amino-6-methyl-4,4a,5,6-tetrahydropyrano[3,4-*d*][1,3]thiazin-8a(8h)-yl-1,3-thiazol-4-yl) Amides as Inhibitors of Beta-site Amyloid Precursor Protein Cleaving Enzyme 1 (BACE1). WO 2015155626A1, Oct 15, 2015.

(26) May, P. C.; Willis, B. A.; Lowe, S. L.; Dean, R. A.; Monk, S. A.; Cocke, P. J.; Audia, J. E.; Boggs, L. N.; Borders, A. R.; Brier, R. A.; Calligaro, D. O.; Day, T. A.; Ereshefsky, L.; Erickson, J. A.; Gevorkyan, H.; Gonzales, C. R.; James, D. E.; Jhee, S. S.; Komjathy, S. F.; Li, L.; Lindstrom, T. D.; Mathes, B. M.; Martenyi, F.; Sheehan, S. M.; Stout, S. L.; Timm, D. E.; Vaught, G. M.; Watson, B. M.; Winneroski, L. L.; Yang, Z.; Mergott, D. J. The potent BACE1 inhibitor LY2886721 elicits robust central A β pharmacodynamic responses in mice, dogs, and humans. *J. Neurosci.* **2015**, *35*, 1199–1210.

(27) Zhang, L.; Chen, L.; Beck, E. M.; Chappie, T. A.; Coelho, R. V.; Doran, S.; Fan, K. – H.; Helal, C. J.; Humphrey, J. M.; Hughes, Z.; Kuszpit, K.; Lachapelle, E. A.; Lazzaro, J. T.; Lee, C.; Mather, R. J.; Patel, N. C.; Skaddan, M. B.; Sciabola, S.; Verhoest, P. R.; Young, J. M.; Zasadny, K.; Villalobos, A. The discovery of a novel phosphodiesterase (PDE)4B-prefering radioligand for positron emission tomography (PET) imaging. *J. Med. Chem.* **2017**, *60*, 8538–8551.

(28) Butler, C. R.; Brodney, M. A.; Beck, E. M.; Barreiro, G.; Nolan, C. E.; Pan, F.; Vajdos, F.; Parris, K.; Varghese, A. H.; Helal, C. J.; Lira, R.; Doran, S. D.; Riddell, D. R.; Buzon, L. M.; Dutra, J. K.; Martinez-Alsina, L. A.; Ogilvie, K.; Murray, J. C.; Young, J. M.; Atchison, K.; Robshaw, A.; Gonzales, C.; Wang, J.; Zhang, Y.; O'Neill, B. T. Discovery of a series of efficient, centrally efficacious BACE1 inhibitors

through structure-based drug design. *J. Med. Chem.* **2015**, *58*, 2678–2702.

(29) Kalvass, J. C.; Maurer, T. S. Influence of nonspecific brain and plasma binding on CNS exposure: implications for rational drug discovery. *Biopharm. Drug Dispos.* **2002**, *23*, 327–338.